In situ TEM heavy ion irradiation-induced precipitation in an austenitic stainless steel (AISI-348)

Matheus A. Tunes[a,*], Cláudio G. Schön[b], Graeme Greaves[a]

[a]*School of Computing and Engineering, University of Huddersfield, Queensgate, HD1 3DH, United Kingdom*
[b]*Department of Metallurgical and Materials Engineering, University of São Paulo, Brazil*

Abstract

Radiation-induced precipitation was examined in an Nb-stabilised austenitic stainless steel (AISI-348) under heavy ion irradiation *in situ* within a transmission electron microscope (TEM) at 1073 K. Selected-area electron diffraction (SAED), bright- and dark-field TEM were used to investigate the nature of the precipitates within the austenite phase (γ-Fe). The precipitates were confirmed to be of $Cr_{23}C_6$ crystal structure. Therefore, the results herein reported indicate that inert gas bubbles may accelerate clustering and precipitation kinetics in the austenite phase during irradiation.

Keywords: Austenitic Stainless Steels, Radiation Damage, Radiation Induced Precipitation, Heavy ion irradiation *In situ* within a TEM, AISI-348

Austenitic stainless steels have been widely applied in both nuclear and conventional electric power generation plants as well as in chemical and petroleum industries due to mainly their favourable corrosion resistances at high temperatures and suitable mechanical properties [1–6]. In particular, the exposure of the γ-Fe phase in extreme environments of nuclear reactors contributes to the degradation of several properties as energetic particle irradiation modifies the crystal structure by displacing atoms from their lattice positions. Additionally, due to their extensive engineering database, market availability and lower cost compared with other metals and alloys, the austenitic stainless steels are under active consideration to be used as structural materials for nuclear fusion reactors [7, 8]. For these reasons, the stability of the γ-Fe phase under irradiation is an important subject of investigation aiming at mitigating the occurrence of severe degradation mechanisms such as radiation-induced precipitation (RIP) and segregation (RIS).

RIP has been accounted as an important effect of displacive irradiation in austenitic stainless steels [9–11]. The RIP phenomenon is often associated with the degradation of mechanical properties that may lead the steel into fracture under the envelope conditions of LWRs operation [12]. Different precipitates may nucleate and grow within a degraded γ–Fe matrix after neutron exposure [9]. Most frequently occurring are the $M_{23}C_6$ (τ) and M_6C (η) carbides where M stands for a solute element [9, 10].

*Corresponding author: Tel. + 44 01484 472111
Email address: m.a.tunes@hud.ac.uk (Matheus A. Tunes)

Garner *et al.* recently reviewed the formation of $M_{23}C_6$ precipitates as a result of neutron irradiation in the AISI-304 microstructure up to 21.7 dpa at around of 650 K[13]. According to Maziasz [9], further analytical screening often reveal that such neutron-irradiation induced precipitates were Ni- and Si-rich, however, the thermally aged precipitates in the same steels were Ni- and Si-depleted. Maziasz [14] also reported on the formation of M_6C under neutron exposure within the temperature range from 643 to 953 K in the AISI-316 steel. The phase was Ni- and Si-rich either after irradiation or annealing. Yang *et al.* [15–17] have also identified Ni- and Si-rich $M_{23}C_6$ under neutron irradiation of the AISI-348 steel at temperatures around of 973 K. Differences in elemental composition and crystal structure between the irradiation-induced and thermally-induced precipitates consolidated a methodology to assess under which conditions such carbides may form within the context of nuclear materials technology.

Ion beam technology has allowed investigations on the RIP phenomenon to be carried out in either *ex situ* or *in situ* within a TEM. Due to the limited worldwide availability of materials test reactors as well as the high costs and hazards associated with post-neutron-irradiation tests, irradiation experiments with ion beams (specially with heavy ions [18, 19]) have shed light on fundamental aspects of precipitation in these complex multicomponent Fe-based alloys. Recently, Jin *et al.* observed the formation of $Cr_{23}C_6$ after *ex situ* TEM ion irradiation with 120 keV Ar ions at 823 K in the system Fe-24.8Cr-19.7Ni-0.4Mn-0.4Nb (weight percent or %wt.), commercially known as HR3C steel [12]. Crystallographic indexing was used to confirm the τ precipitates. The authors also showed that upon increasing the dose, the $Cr_{23}C_6$ grew in size as well as its areal density within the γ-Fe matrix. Interestingly, these authors found that under such irradiation conditions and temperature, the formation of $Cr_{23}C_6$ precipitates was prone to occur specially closer and inside dislocation loops (likely formed prior to RIP, but during irradiation) which had acted as sinks for irradiation-induced segregated solute elements [12].

To date, such electron microscopy investigations have been carried out with austenitic steel specimens after either neutron or ion bombardment. The microstructural response of an austenitic stainless steel under heavy ion irradiation *in situ* within a TEM was investigated in this work. The technique allowed the real-time observation of nucleation and growth of precipitates throughout the γ-Fe matrix with concurrent observation of inert gas bubbles: the latter also an important degradation mechanism within the technology of nuclear materials [20].

The alloy studied was the commercial austenitic stainless steel AISI-348. This steel has particular relevance to the nuclear field as the addition of Nb and Ta improves its corrosion resistance at high temperatures by removing C from solid solution during synthesis and processing [2, 3]. The AISI-348 also lacks of irradiation data in scientific literature according to Garner *et al.* [6]. Inductively coupled plasma optical emission spectrometry (ICP-OES) technique showed that the bulk alloy has **Fe**-17.50**Cr**-9.47**Ni**-1.81**Mn**-0.32**Nb**-0.037**C**-0.001**S**-0.002**P**-0.001**Co**-0.008**B**-0.003**Ta** (%wt.) in solid solution. The specimens were grinded and polished with SiC papers with grits from 120 to 1200 aiming at reducing their initial thicknesses. Then, 3 mm disks were punched and electropolished using a Struers TenuPol-5 with an

electrolyte composed of 90% perchloric acid ($HClO_4$) and 10% (vol.%) of methanol (CH_3OH) at a bath temperature of 233 K. The electropolishing was performed until perforation and samples were washed several times in methanol and dried in air.

The irradiations were carried out in the MIAMI-1 facility at University of Huddersfield. The facility consists of a JEOL JEM-2000FX operating at 200 kV coupled with an 100 kV ion implanter [21, 22]. Images and videos were recorded using a Gatan ORIUS SC200 digital camera. Specimens were irradiated with 30 keV Xe ions at 1073 K ($0.56T_m$) using a Gatan double-tilt heating holder. Heavy ion irradiation is an acknowledged methodology to assess the radiation resistance of Fe and Fe-based alloys [23]. Samples were annealed at 1073 K during 20 min before the experiments. Calculations using SRIM-2013 showed that, for such irradiation conditions, the implantation peak was around of 10 nm and an average of 355 vacancies were estimated per ion collision. At the specimen position within the TEM, the ion flux was measured to be 3.8×10^{13} ions·cm^{-2}·s^{-1}. Using a recent procedure suggested by Stoller *et .al* [24] it was possible to convert the fluences to dpa (displacement-per-atom). Under these conditions, a fluence of $3.6{\times}10^{15}$ ions·cm^{-2} corresponds to 1.3 dpa and, similarly, a fluence of $2.0{\times}10^{16}$ ions·cm^{-2} corresponds to 7.3 dpa.

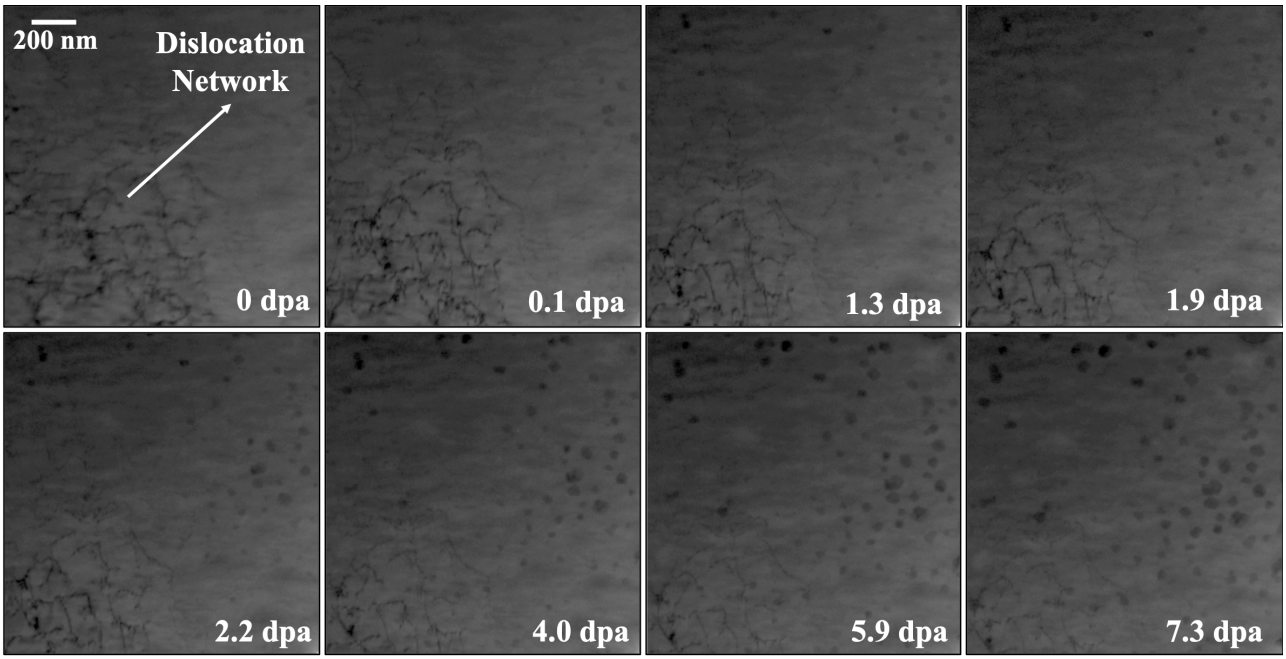

Figure 1: A set of BFTEM micrographs showing the real-time microstructural evolution of the γ-Fe under 30 keV Xe heavy ion irradiation at 1073 K from 0 to 7.3 dpa. Note: scale marker in the first image applies to all micrographs in the figure. The field of view varies slightly due to both thermal and irradiation drifts.

A set of bright-field transmission electron microscopy (BFTEM) micrographs extracted from the *in situ* TEM ion irradiation experiment at 1073 K is shown in the figure 1. Small particles with sizes around of 2-5 nm were initially observed to nucleate at the early stages of the irradiation with doses as low as 0.1 dpa. Upon increasing the irradiation dose, the precipitates grew as can be noticed by the significant changes in the bright-field contrast around the precipitates. However, above 5.9 dpa, the precipitates stopped to grow significantly. Additionally, the dislocation network (in the bottom left side of the images) seemed to undergo into annihilation upon

increasing the irradiation dose. This is noticiable when comparing the microstructures at 0 and 7.3 dpa. The nucleation and growth of precipitates occurred preferentially in the surroundings of the dislocation network and not within it. It is important emphasising that such dislocation network was present before irradiation and remained stable after the annealing up to 1073 K.

TEM characterisation of the AISI-348 before and after the heavy ion irradiation is shown in figure 2 where the microstructure before irradiation and after 20 minutes of annealing at 1073 K is shown in the figure 2(a). Figure 2(b) shows the same area after 17 dpa where precipitates can be observed uniformly distributed along the γ-Fe phase. Figure 2(c) is a selected-area micrograph with some precipitates close to the edge of the irradiated specimen. Its respective diffraction pattern is in figure 2(d). The small inset in figure 2(c) shows a DFTEM micrograph revealing that the precipitates are responsive to diffraction contrast. A crystallographic model simulated with the CrystalMaker software and with data available in the scientific literature for the $Cr_{23}C_6$ crystal structure [25] is shown in the figures 2(e-f). The experimentally obtained diffraction pattern in figure 2(d) matches with the [010] zone axis of the $Cr_{23}C_6$ cubic structure.

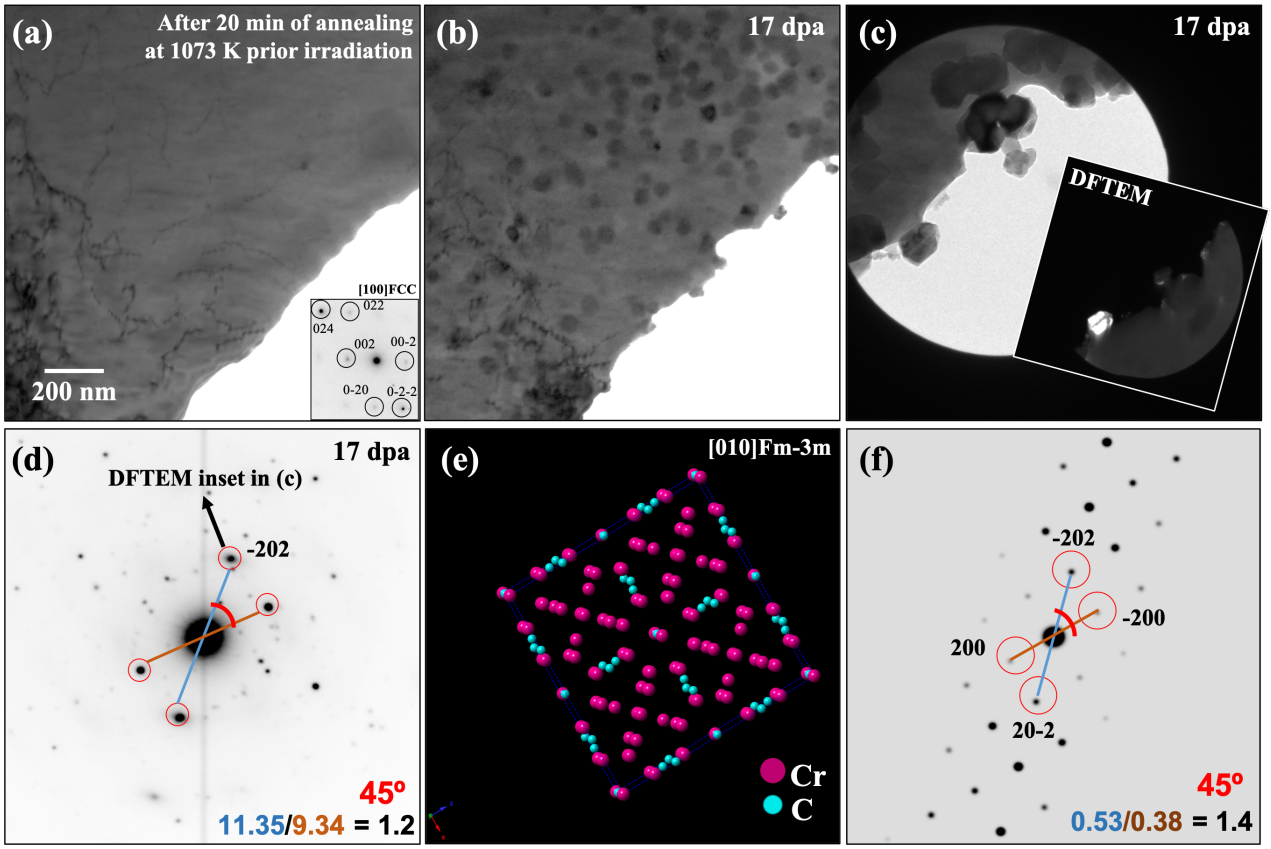

Figure 2: BFTEM micrographs (a) and (b) were taken in a same area before and after irradiation at 17 dpa, respectively. Micrograph (c) is a SAED micrograph with (d) its respective diffraction pattern at 17 dpa. The small inset in (c) corresponds to a DFTEM micrograph from the same area. With crystallographic data from literature [25] the CrystalMaker model for the $Cr_{23}C_6$ precipitates is presented in images (e) corresponding to the zone axis [010] and (f) the respective simulated diffraction pattern.

Post-irradiation characterisation at 20 dpa shows Xe bubbles within the γ-Fe matrix as shown in the BFTEM micrograph in figure 3(a). The zoomed region in figure 3(b) shows that the precipitates were observed in regions where Xe bubbles were also detected. The profile in figure 3(c) exhibits contrast differences among precipitates, bubbles and the austenite matrix.

Precipitates and matrix are of diffraction contrast while inert gas bubbles can be detected by means of through-focal imaging (Fresnel contrast) [26]. The average bubble size was measured within the ImageJ to be 10.5±3.2 nm. Similarly, precipitates had an average final length of 30.7±4.5 nm at 20 dpa.

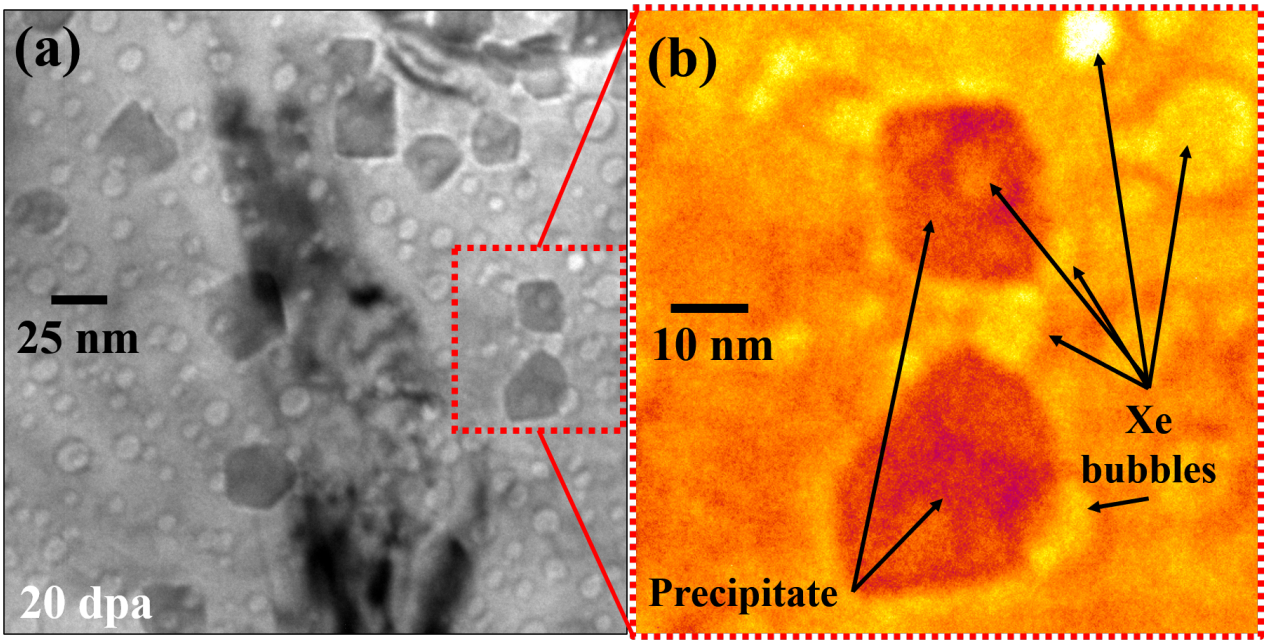

Figure 3: Underfocused (1 μm of defocus degree) BFTEM micrograph (a) showing the precipitates and Xe bubbles along the γ-Fe microstructure after 20 dpa. The image (b) is a zoom from the dashed rectangle in (a): the image was coloured within the ImageJ for better visualisation purposes.

Past studies on radiation behaviour of multicomponent alloys showed that the generation of Frankel defects (i.e. vacancies and interstitials) at supersaturated levels contributes to enhance solute diffusion: the radiation-enhanced diffusion (RED) effect [27, 28]. In austenitic stainless steels, Cr is known to be the most diffusive element which segregates preferentially at grain boundaries and dislocations [28]. The radiation-induced segregation (RIS) effect triggered by RED lowers the Gibbs free energy steel by means of eliminating concentration gradients which favours nucleation and growth of secondary phases like as the $Cr_{23}C_6$. As the atomic diffusivity is faster under irradiation, precipitation is then accelerated when compared with thermal annealing. $Cr_{23}C_6$ were reported to form in the 18Cr-12Ni (%wt.) steel after 80 h of thermal treatment at 923 K and under stress [3]. Similarly, in an austenitic stainless steel with supersaturation of Cr, like the HR3C [12], precipitation of $Cr_{23}C_6$ start to occur only after around of 500 h at 973 K.

Herein, $Cr_{23}C_6$ precipitates were tracked to nucleate within the AISI-348 austenitic matrix immediately upon starting the heavy ion irradiation at a dose level of approximately 0.1 dpa. In a very similar work, but using *ex situ* heavy ion irradiation and TEM, Jin *et al.* [12] reported on formation of Cr carbides at 4.8 dpa in the HR3C austenitic steel. Similarly, we have confirmed that there is a direct relationship between dose, precipitates size and areal density, as can be seen directly in figure 1, but the precipitates stopped to grow significantly at around of 4.0 dpa. Shrink or dissolution of such precipitates were not noticed in the experiments reported in this

work, indicating a certain degree of stability upon the continuous irradiation at an intermediate temperature (*i.e.* 1073 K). Regarding the heavy irradiations on the HR3C steel reported by Jin *et al.* [12], the average final length after 28.8 dpa was approximately 8.2 nm. Comparing the Cr content in the HR3C ($\approx$ 25 %wt.) and the AISI-348 ($\approx$ 18 %wt.) steels, one can see that the first is supersaturated in Cr. As this element is often reported to be the most diffusive element in austenitic stainless steels under irradiation [28], in the HR3C experiment, the rate of Cr diffusion into γ-Fe phase may be higher than in the 30 keV Xe irradiated AISI-348. This promotes greater precipitation density which suppress the grow which may explain the differences on precipitates size between the work by Jin *et al.* and this current work.

DFTEM and SAED micrographs in figure 2 have proven to be a suitable methodology to confirm the crystal structure of the irradiation-induced precipitates. This has been also confirmed in previous similar studies [12]. The crystallographic indexing in figure 2(d-f) shows that the experimental diffraction pattern matches well with the cubic $Cr_{23}C_6$ zone axis [010] from data in literature [25].

Whilst for Jin *et al.* [12] the $Cr_{23}C_6$ precipitates were formed within dislocation loops and lines, this current work showed that RIP was preferentially observed within the degraded γ-Fe grains. Clearly, the pre-existing dislocation network in figure 1 was not a site where precipitation has significantly occurred. Conversely, post-irradiation characterisation at 20 dpa demonstrated that Xe bubbles were observed in regions where precipitates have nucleated and grown (figure 3). Although TEM micrographs do not confirm that an inert gas bubble is touching a precipitate, the nucleation of inert gas bubbles creates surfaces that may contribute as specific site dependencies for segregation of alloying elements under irradiation. This may result in a favourable site for nucleation of secondary phases [9, 10]. Either this work and the one reported by Jin *et al.* [12] are indicating that heavy ion irradiation at high temperatures have led the γ-Fe phase to an instability region where the austenite starts to decompose and lose structural integrity, as the nucleation of precipitates is a well known contributor for embrittlement of steels. Additionally, the supersaturation of point defects generated by heavy ion irradiation together and the subsequent RED effect are clearly acting to change the kinetics of $Cr_{23}C_6$ precipitation in austenitic steels. In this way, RED is the main cause for the acceleration of ageing in such steels.

RIS and RIP in austenitic stainless steels can be interpreted as a non-equilibrium thermodynamic process in which the competition between the recombination of vacancies and interstitials (lower irradiation temperature range), alloying elements segregation and back diffusion of vacancies (higher irradiation temperature range) at dose rates ranging from 10^{-6} to 10^{-2} dpa$\cdot$s^{-1} and irradiation temperature range from 0.1 to 0.8T_m (where T_m is the melting temperature of the alloy) will define whether segregation is prone to occur or not [29–34]. By this, it is worth emphasising that the irradiation conditions reported in this work – i.e. dose rate of 1.4×10^{-2} dpa$\cdot$s^{-1} at 1073 K – lie within the thresholds proposed by Wiedersich-Okamoto-Lam *et al.* [33, 34] where either RIS and RIP are prone to occur in austenitic stainless steels. This present work also shows that inert gas bubbles, when nucleated, may play a major rule in these

processes as it affects the dynamics of nucleation by creating surfaces that act as sinks for solute segregation [35] and *embryo* nucleation and growth. In this sense, the presence of extended defects such as cavities and bubbles as well as dislocation loops introduced by irradiation should be taken into consideration in these earlier RIS and RIP models.

In this work, to the best of our knowledge, we report for the first time the real-time observation of RIP in the AISI-348 under heavy ion irradiation. The crystalline nature of the precipitates was assessed by means TEM characterisation and with the crystallographic data available in literature. We found a direct relationship between dose, precipitates size and areal density, although at around 4.0 dpa further growth was suppressed and the precipitates were observed to be stable under irradiation at around of 20 dpa. The final average length for the precipitates was 30.7±4.5 nm at 20 dpa. RIP has not occurred preferentially at dislocation loops or lines as previously reported [12], but there is scientific evidence that the nucleation and growth of inert gas bubbles may be promote precipitation, therefore further accelerating the alloy ageing under irradiation. Another important conclusion that can be drawn from the results shown in this paper with respect to the metallurgy of austenitic stainless steels is that the Nb addition in the AISI-348 was found to be not sufficient to prevent (or delay) such observed precipitation. Additional studies on the elemental composition of irradiation-induced precipitates are needed to compare with those precipitates observed in thermal annealed microstructures.

Acknowledgements

The authors are grateful to the Engineering and Physical Sciences Research Council (EPRSC) for funding MIAMI-1 facility (grant number EP/E017266/1). The authors are grateful to Dr. Robert W. Harrison (University of Manchester) for useful discussions on the paper and Dr. Nathanael W. S. Moraes (University of São Paulo) for cross-checking the composition of the AISI-348 steel. CGS acknowledges the financial support by the Brazilian National Research, Development and Innovation Council (CNPq, Brasília, Brazil) under the grant number 308565/2018-5. MAT would like to thank Professor Stephen E. Donnelly (University of Huddersfield) and Dr. Philip D. Edmondson (Oak Ridge National Laboratory) to support his doctoral research.

References

[1] G. E. Lucas, Journal of Nuclear Materials 206 (1993) 287–305. URL: http://www.sciencedirect.com/science/article/pii/002231159390129M. doi:10.1016/0022-3115(93)90129-M.

[2] T. Sourmail, Materials science and technology 17 (2001) 1–14.

[3] H. Bhadeshia, R. Honeycombe, Steels Microstructure and Properties, Butterworth-Heinemann, 2017.

[4] F. Garner, B. Oliver, L. Greenwood, Journal of Nuclear Materials 258-263 (1998) 1740–1744. URL: http://linkinghub.elsevier.com/retrieve/pii/S0022311598002979. doi:10.1016/S0022-3115(98)00297-9.

[5] F. Garner, in: Materials Science and Technology, Wiley-VCH Verlag GmbH & Co. KGaA, Weinheim, Germany, 2006. URL: http://doi.wiley.com/10.1002/9783527603978.mst0110. doi:10.1002/9783527603978.mst0110.

[6] F. A. Garner, L. R. Greenwood, R. E. Mizia (2007). doi:10.2172/923501.

[7] S. Şahin, M. Übeyli, Journal of fusion energy 27 (2008) 271–277.

[8] A. Tavassoli, Fusion Engineering and Design 29 (1995) 371–390.

[9] P. Maziasz, P.J., Effects of helium content of microstructural development in Type 316 stainless steel under neutron irradiation, Technical Report, Oak Ridge National Laboratory (ORNL), Oak Ridge, TN (United States), 1985. URL: http://www.osti.gov/servlets/purl/6441891-1MVi1A/. doi:10.2172/6441891.

[10] P. J. Maziasz, C. J. McHargue, International Materials Reviews 32 (1987) 190–219. URL: http://www.tandfonline.com/doi/full/10.1179/095066087790150331. doi:10.1179/095066087790150331.

[11] J.-H. Shim, E. Povoden-Karadeniz, E. Kozeschnik, B. D. Wirth, Journal of Nuclear Materials 462 (2015) 250 – 257. URL: http://www.sciencedirect.com/science/article/pii/S0022311515002159. doi:https://doi.org/10.1016/j.jnucmat.2015.04.013.

[12] S. Jin, L. Guo, F. Luo, Z. Yao, S. Ma, R. Tang, Scripta Materialia 68 (2013) 138–141. URL: http://dx.doi.org/10.1016/j.scriptamat.2012.10.002. doi:10.1016/j.scriptamat.2012.10.002.

[13] F. Garner, in: Comprehensive Nuclear Materials, 1, Elsevier, 2012, pp. 33–95. URL: http://linkinghub.elsevier.com/retrieve/pii/B9780080560335000653. doi:10.1016/B978-0-08-056033-5.00065-3.

[14] P. J. Maziasz, Scripta Metallurgica 13 (1979) 621–626. URL: http://www.sciencedirect.com/science/article/pii/0036974879901212. doi:10.1016/0036-9748(79)90121-2.

[15] W. Yang, H. Brager, F. Garner, Radiation-induced phase development in AISI 316, Technical Report, Hanford Engineering Development Lab., Richland, WA (USA), 1980.

[16] W. Yang, F. Garner, Relationship between phase development and swelling of AISI 316 during temperature changes, ASTM International, 1982.

[17] W. Yang, H. Brager, F. Garner, The Metallurgical Society of AIME, Warrendale, PA (1981) 257.

[18] C. English, B. Eyre, M. Jenkins, Nature 263 (1976) 400.

[19] M. Jenkins, C. English, B. Eyre, Philosophical Magazine A 38 (1978) 97–114.

[20] S. E. Donnelly, J. H. Evans, Fundamental aspects of inert gases in solids, volume 279, Springer, 2013.

[21] J. Hinks, J. Van Den Berg, S. Donnelly, Journal of Vacuum Science & Technology A: Vacuum, Surfaces, and Films 29 (2011) 021003.

[22] G. Greaves, A. Mir, R. Harrison, M. Tunes, S. Donnelly, J. Hinks, Nuclear Instruments and Methods in Physics Research Section A: Accelerators, Spectrometers, Detectors and Associated Equipment 931 (2019) 37–43.

[23] C. A. English, B. L. Eyre, Nature 260 (1976) 619–21. URL: http://www.ncbi.nlm.nih.gov/pubmed/1264226. doi:10.1038/260170a0.

[24] R. E. Stoller, M. B. Toloczko, G. S. Was, A. G. Certain, S. Dwaraknath, F. A. Garner, Nuclear Instruments and Methods in Physics Research Section B: Beam Interactions with Materials and Atoms 310 (2013) 75–80. URL: http://www.sciencedirect.com/science/article/pii/S0168583X13005053. doi:10.1016/j.nimb.2013.05.008.

[25] A. L. Bowman, G. P. Arnold, E. K. Storms, N. G. Nereson, Acta Crystallographica Section B Structural Crystallography and Crystal Chemistry 28 (1972) 3102–3103. URL: http://scripts.iucr.org/cgi-bin/paper?S0567740872007526. doi:10.1107/S0567740872007526.

[26] S. E. Donnelly, Radiation Effects 90 (1985) 1–47. URL: http://www.tandfonline.com/doi/abs/10.1080/00337578508222514. doi:10.1080/00337578508222514.

[27] J. A. Brinkman, W. Wiedersich, in: Flow and fracture of metals and alloys in nuclear environments, ASTM International, Philadelphia, 1965, pp. 3–39. URL: http://www.astm.org/doiLink.cgi?STP43520S. doi:10.1520/STP43520S.

[28] T. R. Anthony, in: J.W. Cobertt and L.C. Ianniello (Ed.), Radiation-induced voids in metals, volume 15, USAEC CONF-710601, 1971, pp. 630–646. URL: http://www.dtic.mil/docs/citations/AD0732507.

[29] R. Faulkner, S. Song, D. Meade, C. Goodwin, in: Materials Science Forum, volume 294, pp. 67–74.

[30] E. Kenik, T. Inazumi, G. Bell, Journal of Nuclear Materials 183 (1991) 145–153.

[31] R. Carter, D. Damcott, M. Atzmon, G. Was, S. M. Bruemmer, E. Kenik, Journal of Nuclear Materials 211 (1994) 70–84.

[32] S. M. Bruemmer, L. A. Charlot, J. S. Vetrano, E. P. Simonen, MRS Proceedings 373 (1994) 119. doi:10.

1557/PROC-373-119.

[33] P. R. Okamoto, L. E. Rehn, Journal of Nuclear Materials 83 (1979) 2–23. doi:10.1016/0022-3115(79)90587-7.

[34] H. Wiedersich, P. Okamoto, N. Q. Lam, Journal of Nuclear Materials 83 (1979) 98–108.

[35] B. Kombaiah, K. Jin, H. Bei, P. D. Edmondson, Y. Zhang, Materials & Design 160 (2018) 1208–1216.